www.czasopisma.pan.pl PAN www.journals.pan.pl
Chemical and Process Engineering 2021, 42 (3), 223–234
DOI: 10.24425/cpe.2021.138927

PHENOMENOLOGICAL AND NUMERICAL ISSUES CONCERNING DYNAMICS OF NONISOBARIC MULTICOMPONENT DIFFUSION OF GASES IN MACROPOROUS MEDIA

Katarzyna Bizon*, Bolesław Tabiś

Cracow University of Technology, Faculty of Chemical Engineering and Technology,
ul. Warszawska 24, 31-155 Kraków, Poland

The study addresses two groups of issues occurring in modeling and experimental studies of multicomponent nonisobaric diffusion in macroporous materials. The dynamics of such processes is described in terms of systems of nonlinear partial differential equations. A method of orthogonal collocation for resolving the equations is proposed and compared with the method of lines. The second group of problems presented involves numerical simulations of diffusion in a Wicke–Kallenbach diffusion cell. Such an apparatus is used in experimental studies. Particular attention is paid to diffusion in a cell closed from both sides. This is an analogue of the Duncan–Toor experiment. The effect of the number of diffusing components and their initial concentrations on the dynamics of diffusion in binary and ternary solution was studied. Hitherto unknown dynamic properties of such processes were detected and discussed.

Keywords: multicomponent diffusion, porous media, dynamics

1. INTRODUCTION

Porous materials play an unquestionable role in many operations and processes of chemical engineering and technology, in allied industries, in chemical analytics and environmental protection (Krishna and Wesselingh, 1997). They represent a diversified group of solids in terms of morphology, pore size, and chemical properties. Their technical applications appear to be equally abundant. Well-known processes involving porous media include adsorption, chromatography, drying, an important group of catalytic processes and membrane technologies. All of these processes are accompanied by internal diffusive mass transport.

The quantitative description of diffusive mass transport in porous media is much more challenging than the description of diffusion in fluids. It is associated with the interaction of the solid with the diffusing molecules of the components. This interaction depends on the ratio of the mean free path of molecules to the pore diameter and on the relationship between the sizes of the molecules and the pores. These two relationships are superimposed on the thermodynamic features of the process, i.e. the interfacial

* Corresponding author, e-mail: katarzyna.bizon@pk.edu.pl

equilibrium and the boiling points of the diffusing components. This gives a great diversity of mechanisms for mass transport in porous materials.

The nonisobaric nature of diffusive mass transport indicates that the total pressure p varies either with time or is a function of spatial coordinates, or both. This phenomenon can originate from different sources. The first is the difference in pressure on both sides of a porous membrane, which is encountered both in industrial practice and in laboratory studies. The reasons for nonisobaric diffusion may also result from the character of the process itself within the porous material. These include nonequimolar chemical reactions leading to an increase or decrease in the total number of moles, sorption phenomena on the internal surface of the solid that also cause changes in the number of moles in the bulk phase, or different rates of diffusion of individual components. Differences in pressure within a porous material result in additional mass transport called viscous or convective flow.

For the quantitative description of diffusive mass transport in macroporous materials, i.e. with pore diameters above $5 \cdot 10^{-8}$ m, the dusty gas model is now generally adopted (Ho and Webb, 2006; Krishna and Wesseling, 1997; Mason an Malinauskas, 1983). The validity of this model has been proved empirically many times. Good examples are the experimental works of Veldsink et al. (1994), Remick and Geankoplis (1970), Remick and Geankoplis (1974) and Yang et al. (2005). These references give a description of the experimental setups and measurement methods so that they can be easily reproduced in other laboratories.

2. NONISOBARIC DIFFUSION MODEL AND METHOD OF STUDYING THE DYNAMICS

Let there be transient diffusion in a porous material in a gaseous mixture containing K components. The dusty gas model commonly used to describe diffusion in porous media originates from the Maxwell–Stefan equations (Krishna and Wesseling, 1997). The solid that the gas molecules interact with is treated as huge spheres with infinite mass and zero velocity, representing the $K + 1$ component in the diffusion system. A mathematical model of the mass transport is derived based on conservation laws related to the differential volume dV (Fig. 1).

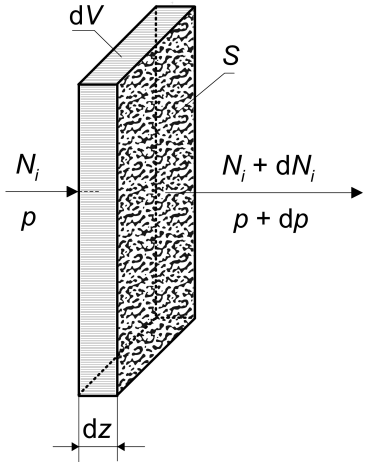

Fig. 1. A representative differential volume of a porous body with planar geometry and fundamental notations

We analyze the mass transport in macroporous materials for gaseous components not subject to adsorption. For the i^{th} component of the mixture we obtain then the following mass balance

$$\frac{\partial n_i}{\partial t} = SN_i(z) - S\left[N_i(z) + \frac{\partial N_i(z)}{\partial z}\mathrm{d}z\right] = -S\frac{\partial N_i(z)}{\partial z}\mathrm{d}z \tag{1}$$

Despite the fact that mass transport takes place only through the pores, the molar fluxes N_i refer to the entire surface area S. This is because the pore contribution is taken into account in the definition of the effective molecular and Knudsen diffusion coefficients and in the permeability coefficient.

The left-hand side of the mass balance (1) is the mass accumulation rate of the i^{th} component in the pores, where n_i is

$$n_i = S\varepsilon \frac{p_i}{RT} \mathrm{d}z \quad (i = 1, 2, ..., K) \tag{2}$$

Using matrix notation, Eqs. (1) and (2) can be written as

$$\frac{\varepsilon}{RT} \frac{\partial \mathbf{p}}{\partial t} = -\frac{\partial \mathbf{N}}{\partial z} \tag{3}$$

In Eq. (2) $\mathbf{N}$ is the molar flux vector. If the diffusion is nonisobaric, then

$$\mathbf{N} = -\frac{1}{RT} \mathbf{B}^{-1}(\mathbf{y}) \frac{\mathrm{d}\mathbf{p}}{\mathrm{d}z} - \frac{\mathcal{B}^e}{RT\eta} \frac{\mathrm{d}p}{\mathrm{d}z} \cdot \mathbf{B}^{-1}(\mathbf{y}) \cdot \mathbf{E} \cdot \mathbf{p} \tag{4}$$

Eq. (4) determines the molar flux of combined molecular diffusion, Knudsen diffusion, and convective flow driven by the total pressure gradient in a given porous material. It is derived from the Maxwell–Stefan model and the Navier–Stokes equation to account for the contribution of convective flow. By introducing expression (4) into Eq. (3) one gets the model of unsteady diffusion

$$\varepsilon \frac{\partial \mathbf{p}}{\partial t} = \frac{\partial}{\partial z} \left[\mathbf{B}^{-1}(\mathbf{y}) \frac{\partial \mathbf{p}}{\partial z} + \frac{\mathcal{B}^e}{\eta} \frac{\partial p}{\partial z} \cdot \mathbf{B}^{-1}(\mathbf{y}) \cdot \mathbf{E} \cdot \mathbf{p} \right] \tag{5}$$

The model consists of a system of K nonlinear partial differential equations in which

$$\mathbf{N} = \left[N_1, N_2, \ldots, N_K \right]^T, \qquad \mathbf{y} = \left[y_1, y_2, \ldots, y_K \right]^T, \qquad \mathbf{p} = \left[p_1, p_2, \ldots, p_K \right]^T \tag{6}$$

and

$$\mathbf{y} = \frac{\mathbf{p}}{p}, \qquad \eta = \eta(\mathbf{y}, p) \tag{7}$$

The following initial conditions are associated with the system of Eq. (5)

$$\mathbf{p}(z, 0) = \boldsymbol{\upsilon}(z); \quad t = 0; \quad z \in [0, L] \tag{8}$$

The boundary conditions can be of different types, i.e. conditions of the first-, second- and third-type, depending on how the diffusion occurs.

The matrices $\mathbf{B}$ and $\mathbf{E}$ in Eqs. (4) and (5) contain the effective molecular and Knudsen diffusion coefficients and are defined as follows

$$\mathbf{B}(\mathbf{y}) = \begin{bmatrix} \displaystyle\sum_{\substack{j=1 \\ j \neq i}}^{K} \frac{y_j}{D^e_{ij}} + \frac{1}{D_{i,Kn}} & \text{for } i = j \\ -\dfrac{y_i}{D^e_{ij}} & \text{for } i \neq j \end{bmatrix}_{K \times K} \tag{9}$$

and

$$\mathbf{E} = \begin{bmatrix} \dfrac{1}{D^e_{Kn,1}} & 0 & \ldots & 0 \\ 0 & \dfrac{1}{D^e_{Kn,2}} & \ldots & 0 \\ \vdots & \vdots & \vdots & \vdots \\ 0 & 0 & 0 & \dfrac{1}{D^e_{Kn,K}} \end{bmatrix}_{K \times K} \tag{10}$$

The above mentioned effective molecular and Knudsen diffusion coefficients are calculated as

$$D^e_{Kn,i} = \frac{\varepsilon}{\tau} D_{Kn,i}, \qquad D_{Kn,i} = \frac{d_p}{3}\sqrt{\frac{8RT}{\pi M_i}} \tag{11}$$

The parameter $\mathcal{B}^e$ is the so-called effective permeability factor of the porous material

$$\mathcal{B}^e = \frac{\varepsilon}{\tau}\frac{d_p^2}{32} \tag{12}$$

If diffusion occurs in a single straight cylindrical capillary or in a bundle of such capillaries, then $\varepsilon/\tau = 1$. The total pressure gradient present in Eq. (5) is calculated as

$$\frac{\mathrm{d}p}{\mathrm{d}z} = -\frac{RT\sum_{i=1}^{K}\frac{N_i}{D^e_{Kn,i}}}{1+\frac{\mathcal{B}^e p}{\eta}\sum_{i=1}^{K}\frac{y_i}{D^e_{Kn,i}}} \tag{13}$$

For isobaric diffusion, this gradient is equal to zero. The model (5) is usually applied to two groups of problems:

- in process calculations involving multicomponent diffusion,
- in experimental studies aimed at identification of model parameters by comparing measured data with results of numerical simulations.

In our own previous works, different versions of model (5) were used for:

- determination of structural parameters of porous materials (Tabiś and Boroń, 2020),
- explanation of the phenomenon of reversal of diffusion fluxes during mass transport through macroporous materials (Boroń and Tabiś, 2020),
- proposal of a method for simultaneous determination of correlated coefficients of molecular diffusion and Knudsen diffusion (Boroń, 2020).

The Wicke–Kalllenbach diffusion cell and its modifications, shown in Fig. 2, are often used in experimental studies. Its suitability for diffusion studies in porous materials has been reported by a number of authors (Arnošt and Schneider, 1995; Tuchlencki et al., 1998; Veldsink et al., 1994; Yang et al., 2005). The advantage of experimental setup based on the idea shown in Fig. 2 is that it can be built and the measurements can be performed in an averagely equipped laboratory. The second advantage is its low price.

The scheme in Fig. 2a shows a continuous flow diffusion cell. It is a both sides open system. The compartments with volumes V_0 and V_L are separated by a porous membrane of thickness L. Media streams of known feed rates and compositions are continuously fed into and discharged from both compartments. In laboratory measurements, an effort is made to ensure that the volumes V_0 and V_L are under intensely mixed conditions. This is done in order to achieve homogeneity of concentrations in the volumes and to minimize the external resistance to mass transport, i.e., at the interface between the solid and the bulk phase. One way to minimize the external transport resistance is to adopt a sufficiently thick porous membrane. Then the external resistance contributions can be neglected in the total resistance to mass transport (Arnošt and Schneider, 1995).

The continuous flow diffusion cell (Fig. 2a) is an extremely versatile system. It can be used for isobaric and nonisobaric measurements. On the other hand, isobaric measurements, i.e. those when $p(0) = p(L)$, give the possibility of both steady-state and transient studies. The presence of blind pores can be detected from transient measurements. These issues are related to the experimentation of diffusive mass transport.

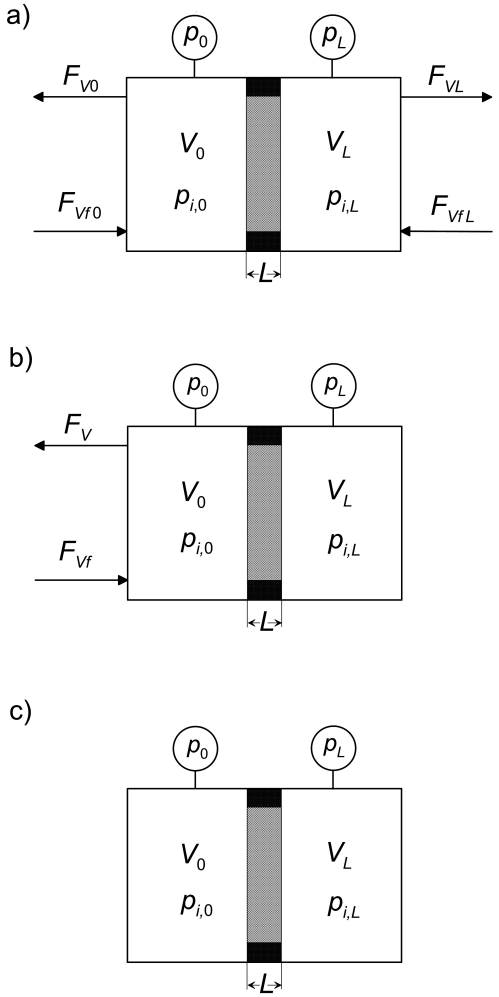

Fig. 2. Three modes of operation of the Wicke–Kallenbach diffusional cell

Diffusion measurements in semi-closed cells, as in Fig. 2b, are also known and practiced. In such systems, transient diffusion measurements are carried out (Veldsink et al., 1994). Let the closed compartment be the one denoted as V_L. The equations to determine the partial pressures for $z = 0$ and for $z = L$ then take the form

$$\frac{V_0}{RT}\frac{\mathrm{d}\mathbf{p}_0}{\mathrm{d}t} = F_{Vf0}\frac{\mathbf{p}_{f0}}{RT} - F_{V0}\frac{\mathbf{p}_0}{RT} - S\mathbf{N}\Big|_{z=0} \tag{14}$$

$$\frac{V_L}{RT}\frac{\mathrm{d}\mathbf{p}_L}{\mathrm{d}t} = S\mathbf{N}\Big|_{z=L} \tag{15}$$

There is a third option for empirical and simulation studies of diffusion dynamics. It involves the use of a two-sided closed Wicke–Kallenbach cell, i.e. as the one shown in Fig. 2c. Then, the partial differential equations of the diffusion dynamics (Eq. (5)) are solved together with two systems of ordinary differential equations

$$\frac{V_0}{RT}\frac{\mathrm{d}\mathbf{p}_0}{\mathrm{d}t} = -S\mathbf{N}\Big|_{z=0} \tag{16}$$

$$\frac{V_L}{RT}\frac{\mathrm{d}\mathbf{p}_L}{\mathrm{d}t} = S\mathbf{N}\Big|_{z=L} \tag{17}$$

Theoretical methods used to study diffusion dynamics consist of multiple solving the system of equations (Eq. (5)). Therefore, for the model (Eq. (5)) to obtain computational utility, efficient algorithms for its resolution must be proposed and tested. Two methods have been proposed to reduce the partial differential

equations (Eq. (5)) to systems of ordinary differential equations. These are: the orthogonal collocation method (Finlayson, 1972) and the method of lines (Schiesser, 1991). The basic principles of orthogonal collocation are well known (Finlayson, 1972). Here we present its practical application to resolve the model (Eq. (5)). Before applying the collocation method, the system of equations (Eq. (5)) was transformed to the expanded form by calculating the derivative of the expression in the brackets of the right-hand side of this system. Keeping in mind that the matrix **E** is constant, we obtain

$$\varepsilon L^2 \frac{\partial \mathbf{p}}{\partial t} = \mathbf{B}^{-1} \frac{\partial^2 \mathbf{p}}{\partial \xi^2} + \left[\frac{\partial}{\partial \xi} \mathbf{B}^{-1} \right] \frac{\partial \mathbf{p}}{\partial \xi} + \frac{\mathcal{B}^e}{\eta} \left\{ \frac{\partial^2 p}{\partial \xi^2} \mathbf{B}^{-1} \mathbf{E} \cdot \mathbf{p} + \frac{\partial p}{\partial \xi} \left[\frac{\partial}{\partial \xi} \mathbf{B}^{-1} \right] \mathbf{E} \cdot \mathbf{p} + \frac{\partial p}{\partial \xi} \mathbf{B}^{-1} \mathbf{E} \frac{\partial \mathbf{p}}{\partial \xi} \right\} \tag{18}$$

The above equation was then recast using orthogonal collocation rules. Details concerning the transformation of the equation are provided in the Appendix.

The orthogonal collocation method appears to be algorithmically complex, but it has been proven to be many times faster than the method of lines. This is due to the final number of approximating differential equations, which is many times smaller in the collocation method.

3. VALIDATION OF THE DIFFUSION MODEL AND SIMULATION STUDIES

Experimental results of nonisobaric diffusion of the gaseous solution $\{A_1, A_2\} = \{He, Ar\}$ through a porous membrane with a pore diameter of $8.88 \cdot 10^{-8}$ m obtained by Veldsink et al. (1994) in a semi-flow apparatus, i.e., according to the scheme in Fig. 2b, were used to verify the model (5), (14) and the applied numerical algorithms (A1)–(A4), (A8)–(A9). The time trajectories obtained from this model were compared with experimental data obtained from two series of measurements involving the flushing of helium from the porous material by argon (Fig. 3a) and the displacement of argon by helium (Fig. 3b). It can be concluded that the results obtained from the numerical simulations reflect the experimental data with sufficient reliability.

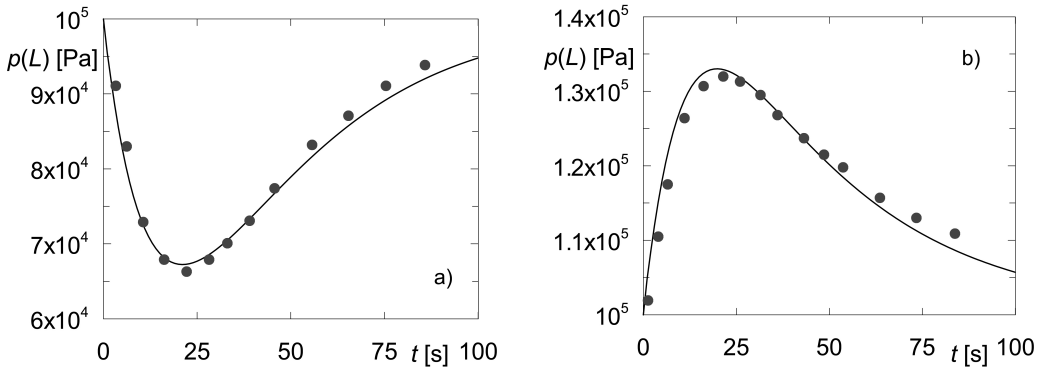

Fig. 3. Experimental validation of the model (5), (14) by simulation of a nonisobaric dynamics with simultaneous molecular and Knudsen diffusion, and with convective flow for two-sided closed diffusion cell (Fig. 2b): (a) helium flushing by argon; (b) argon flushing by helium. Points • originate from binary diffusion measurements {He, Ar} (Veldsink et al., 1994)

In all simulations, orthogonal collocation and the method of lines developed specifically for this purpose (Tabiś and Bizon, 2020) were used to compare the accuracy of the calculations. Seven internal nodes were assumed in the collocation method and the division of the spatial coordinate ξ into one hundred subintervals was adopted in the method of lines. The obtained results then coincide with an accuracy of four significant digits. Such approximation of the dynamics requires solving $K \times 9$ ordinary differential equations following the collocation method, while the method of lines requires as many as $K \times 101$ equations, where K is the

number of diffusing components. For this reason, the collocation method becomes many times faster. The Gear algorithm (Gear, 1971) was employed to integrate the obtained ordinary differential equations. The time trajectories resulting from both methods, reported in this study, are graphically indistinguishable.

The analysis of diffusion in a two-sided closed diffusion cell (Fig. 2c) can be viewed as an analogue of the experiment of Duncan and Toor, who studied the diffusion of ternary gaseous solution (Duncan and Toor, 1962; Tabiś and Bizon, 2018). The experiment of Duncan and Toor concerns isobaric diffusion through a capillary with a diameter several times larger than the pore diameter in a given porous solid. Unlike Duncan and Toor's experiment, in the case of porous media, a simultaneous change in total pressures on both sides of the membrane is observed. This is due to the difference in Knudsen diffusion coefficients of components with significantly different molar masses. Such a phenomenon obtained from the calculation performed for the binary mixture $\{A_1,\ A_2\} = \{He,\ N_2\}$ is shown in Fig. 4. Due to the different operation mode of the diffusion cell, Equations (15) were adopted as boundary conditions.

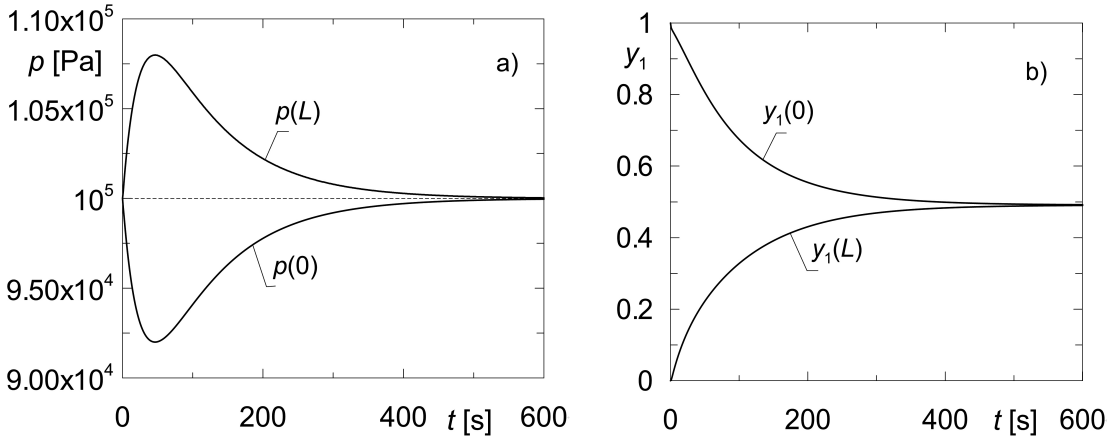

Fig. 4. Changes in total pressure and gas composition in both volumes of the diffusion cell V_0 and V_L during non-isobaric diffusion of a mixture of gases $\{He, N_2\}$ in a closed system (Fig. 2c); $d_p = 5 \cdot 10^{-7}$ m

Initially, the volume V_0 contains helium, the volume V_L contains nitrogen and the pressure in the entire diffusion cell is uniform. As diffusion starts, there is a decrease in total pressure in volume V_0 and an increase in volume V_L. This is due to the higher Knudsen diffusion rate of the component with lower molecular weight, i.e. helium from volume V_0 to V_L. This causes a decrease in the total number of moles in volume V_0 and an increase in volume V_L. As the pressure difference increases, convective flow contributes to a greater extent. Once the pressure extremes are reached in both volumes, there is a gradual decrease in pressure to the value corresponding to the initial time, i.e., $t = 0$, as the concentrations of the two components are equalized throughout the diffusion cell. Such a phenomenon in the Duncan and Toor setup cannot be observed for binary mixtures.

For ternary solution, the situation is more complex. The interesting dynamic phenomena that have been observed for such diffusion depend on the initial composition of the mixtures in volumes V_0 and V_L. These phenomena are discussed below.

Arnold and Toor (1967) investigated the diffusion dynamics in a ternary gas mixture $\{A_1,\ A_2,\ A_3\} = \{CH_4,\ Ar,\ H_2\}$. They used a Loschmidt tube for the measurements. We consider the same ternary system, its physicochemical properties and process conditions to test the model (5) but applied to diffusion through a porous material with a pore diameter $d_p = 10^{-7}$ m, i.e. in the range corresponding to macropores.

Both the Loschmidt tube and the Duncan–Toor two-bulb cell with capillary are two-sided closed systems for which the boundary conditions (Eq. (15)) are satisfied. We therefore simulate the diffusion dynamics

in the system as shown in Fig. 2c, assuming two sets of initial conditions specifying the gas compositions at time $t = 0$ in volumes V_0 and V_L, i.e.:

a) $y_1(0,0) = 0.5$; $y_2(0,0) = 0.5$; $y_3(0,0) = 0$; $y_1(L,0) = 0$; $y_2(L,0) = 0.5$; $y_3(L,0) = 0.5$,
b) $y_1(0,0) = 0.7$; $y_2(0,0) = 0.3$; $y_3(0,0) = 0$; $y_1(L,0) = 0$; $y_2(L,0) = 0.7$; $y_3(L,0) = 0.3$.

The results of dynamic simulations are convenient to illustrate by showing the time trajectories of the molar fractions $y_i(z,t)$ at the points $z = 0$ and $z = L$, i.e. $y_i(0,t)$, $y_i(L,t)$, $(i = 1, 2, \ldots, K)$. The evolution of the total pressure in both volumes $V_0(t)$ and $V_L(t)$ also provides important cognitive and empirical insight, especially since these quantities are easy for being measured frequently.

Fig. 5 shows the dynamic characteristics of three-component nonisobaric diffusion involving methane, argon, and hydrogen for the initial composition in accordance with data set "a". At time $t = 0$, there is a uniform total pressure $p = 10^5$ Pa throughout the diffusion system. The volume V_0 contains an equimolar mixture of methane and argon. In contrast, the volume V_L is charged with an equimolar mixture of argon and hydrogen. It should be noted that initially the argon concentration is kept uniform throughout the entire system.

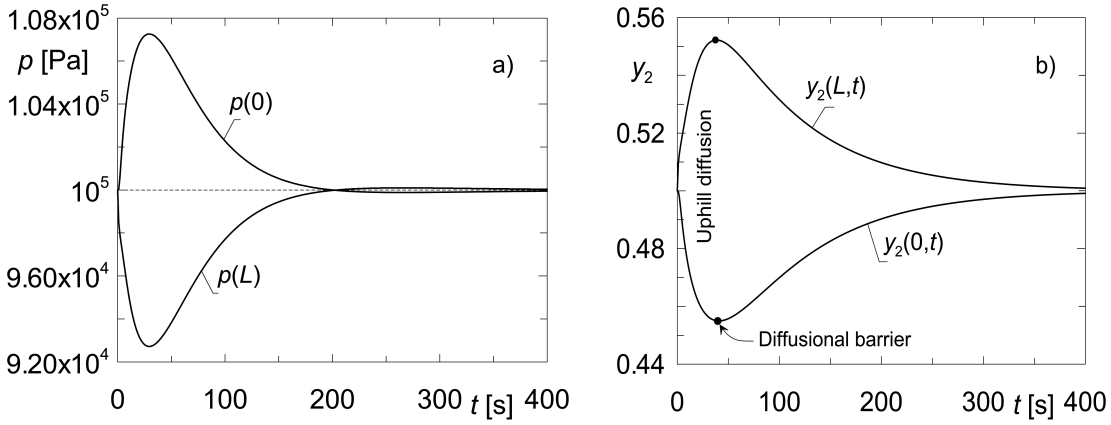

Fig. 5. Time trajectories of the total pressure and molar fractions for the ternary diffusion of $\{A_1, A_2, A_3\} = \{CH_4, Ar, H_2\}$ with initial composition in accordance with set "a" in the two-sided closed system (Fig. 2c); $d_p = 10^{-7}$ m; $L = 10^{-2}$ m; $T = 307$ K

At time $t = 0$, a mutual mass exchange between the two compartments begins due to molecular diffusion, Knudsen diffusion and, as it turns out, also viscous flow. These three mechanisms of mass transport cause unexpected and difficult to predict *a priori* dynamic behavior of the system. As shown in Fig. 5, extremes of both the total pressure in both volumes V_0 and V_L emerge (Fig. 5a) as well as extremes of the molar fraction of the heaviest component, i.e., argon. Moreover, uphill diffusion of this component is observed for the initial period of the process (Fig. 5b). We recall that for $t = 0$, the molar fraction of argon on both sides of the porous membrane was the same, i.e., $y_2(0,0) = y_2(L,0) = 0.5$. From Fig. 5b, we find that the diffusional barrier points on the upper and lower branches of the graph appear at a slightly different time instants. This is due to the difference in gas viscosity on both sides of the membrane.

In Fig. 5a the existence of the second weak extremes of pressure around 260 s from time $t = 0$ can be observed. It was demonstrated that this phenomenon has different degrees of intensity depending on the initial composition of the solutions in volumes V_0 and V_L.

To confirm the existence of multiple pressure extremes, diffusion simulations were performed for the initial gas compositions as shown in set "b". The results are illustrated in Fig. 6. The new phenomenon of the existence of two pairs of total pressure extremes in volumes V_0 and V_L, denoted by $p(0)$ and $p(L)$ in

Fig. 6a, respectively, was confirmed. This phenomenon is likely due to changes in molar flux densities caused by the interaction of molecules having different molar masses and therefore different diffusion rates. However, these pressure extremes do not correspond to uphill diffusion of the component with the highest molecular weight, as shown in Fig. 5b. Instead, it is surprising that this phenomenon transfers to the lightest component (hydrogen), but occurs on a negligibly small scale (Fig. 6b).

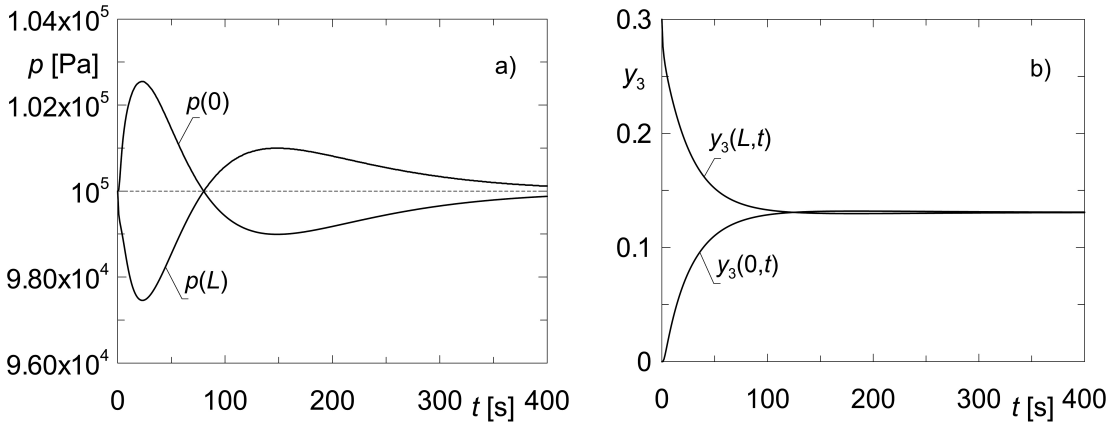

Fig. 6. Time trajectories of the total pressure and molar fractions for the ternary diffusion of $\{A_1, A_2, A_3\} = \{CH_4, Ar, H_2\}$ with initial composition in accordance with set "b" in the two-sided closed system (Fig. 2c); $d_p = 10^{-7}$ m; $L = 10^{-2}$ m; $T = 307$ K

4. CONCLUSIONS

This work concerns the dynamics of the complex process of molecular diffusion, Knudsen diffusion and viscous flow in macroporous solids. The dusty gas model derived from Maxwell–Stefan theory was used for numerical analysis. Two research issues are presented, i.e. a method for solving the equations of diffusion dynamics and simulations of the operation of a Wicke–Kallenbach diffusion chamber under non-isobaric conditions. These are problems encountered in modeling and experimental studies of multicomponent nonisobaric diffusion in macroporous materials.

The presented computational algorithm based on the orthogonal collocation method was tested by comparing the obtained results with the experimental data of Veldsink and co-authors (Veldsink et al., 1994) and with the results derived from numerical simulations based on the method of lines, which is considered to be the reference. The effectiveness and usefulness of the proposed algorithm are demonstrated.

The second issue addressed in this study focuses on the dynamic properties of a closed Wicke–Kallenbach diffusion cell. Such a chamber can be viewed as an analogue of the Duncan–Toor experimental setup. Based on the proposed algorithm, dynamic simulations were performed for binary and ternary gaseous mixtures. Gases not subject to adsorption were chosen to eliminate surface diffusion.

In each of the numerical experiments, the diffusion process was initiated from isobaric conditions, i.e. a uniform total pressure in the system. It has been demonstrated that even for binary diffusion, a pressure difference appears over time and the process progresses in a nonisobaric mode. This is due to the difference in Knudsen diffusion coefficient of the individual components. Once the pressure extremes are reached on both sides of the membrane, a gradual equalization occurs until the initial pressure is reached.

When diffusion proceeds in ternary solutions, then the dynamics of the process depends on the initial composition of the gaseous mixtures on both sides of the porous membrane. Depending on this composition, the following occurs: either reverse diffusion of the component with the highest molar mass or the

phenomenon of multiple total pressure extremes, which has not been reported so far in the literature. The transmission of reverse diffusion from the component with the highest molar mass to the component with the lowest molar mass was also observed but to a small extent. These new phenomena demonstrate that nonisobaric ternary diffusion in porous media constitutes a much more complex process and is more difficult to predict a priori because it introduces new qualitative features.

The proposed method for the simulation of diffusion dynamics has mainly an applicative character, while the demonstrated dynamic phenomena have a fundamental nature.

SYMBOLS

A_i	i^{th} component in the diffusing mixture
b_m	coefficient in the expression for the first derivative according to the Legendre approximation polynomial
$\mathbf{B}$	matrix of diffusion coefficients
$\mathcal{B}^e$	effective permeability coefficient of porous material, m^2
C	total molar concentration, $\mathrm{kmol}\cdot\mathrm{m}^{-3}$
d_p	average pore diameter, m
D_{ij}	binary Maxwell–Stefan diffusion coefficient in the gas phase, $\mathrm{m}^2\cdot\mathrm{s}^{-1}$
$D_{Kn,i}$	Knudsen diffusion coefficient of component i, $\mathrm{m}^2\cdot\mathrm{s}^{-1}$
$\mathbf{E}$	diagonal matrix of the inverse of Knudsen diffusion coefficients, $\mathrm{s}\cdot\mathrm{m}^{-2}$
F_V	volumetric flow rate, $\mathrm{m}^3\cdot\mathrm{s}^{-1}$
g_m	coefficient in the expression for the second derivative according to the Legendre approximation polynomial
L	thickness of the porous membrane, m
m	collocation point index
M	number of internal collocation points
M_i	molecular mass of component i, $\mathrm{kg}\cdot\mathrm{kmol}^{-1}$
N_i	molar flux of component i, $\mathrm{mol}\cdot\mathrm{m}^{-2}\cdot\mathrm{s}^{-1}$
$\mathbf{N}$	vector of molar fluxes, $\mathrm{mol}\cdot\mathrm{m}^{-2}\cdot\mathrm{s}^{-1}$
p	total pressure, Pa
$\mathbf{p}$	vector of partial pressures, Pa
S	cross-section of porous material, m^2
t	time, s
T	temperature, K
u	velocity, $\mathrm{m}\cdot\mathrm{s}^{-1}$
V	volume, m^3
y_i	molar fraction of component i
z	spatial coordinate, m

REFERENCES

Arnold K.R., Toor H.L., 1967. Unsteady diffusion in ternary gas mixtures. *AIChE J.*, 13, 909–914. DOI: 10.1002/aic.690130518.

Arnošt D., Schneider P., 1995. Dynamic transport of multicomponent mixtures of gases in porous solids. *Chem. Eng. J.*, 57, 91–99. DOI: 10.1016/0923-0467(94)02900-8.

Boroń D., 2020. Izobaryczna metoda stacjonarna wyznaczania współczynników dyfuzji w materiałach porowatych. *Przem. Chem.*, 99, 785–788. DOI: 10.15199/62.2020.5.21.

Boroń D., Tabiś B., 2020. Udział i znaczenie przepływu lepkiego w nieizobarycznej dyfuzji gazów przez materiały porowate. *Przem. Chem.*, 99, 1717–1716. DOI: 10.15199/62.2020.12.4.

Duncan J.B., Toor H.L., 1962. An experimental study of three component gas diffusion. *AIChE J.*, 8, 38–41. DOI: 10.1002/aic.690080112.

Finlayson B.A., 1972. *The method of weighted residuals and variational principles.* Academic Press, New York. DOI: 10.1137/1.9781611973242.

Gear C.W., 1971. *Numerical initial value problems in ordinary differential equations.* Prentice-Hall, Englewood Cliffs, New Jersey.

Ho C.K., Webb S.W. (Eds.), 2006. *Gas transport in porous media.* Springer, Netherlands. DOI: 10.1007/1-4020-3962-X.

Krishna R., Wesseling J.A., 1997. The Maxwell–Stefan approach to mass transfer. *Chem. Eng. Sci.*, 52, 861–911. DOI: 10.1016/S0009-2509(96)00458-7.

Mason E.A., Malinauskas A.P., 1983. *Gas transport in porous media: The dusty gas model.* Elsevier, Amsterdam.

Remick R.R., Geankoplis C.J., 1970. Numerical study of three-component gaseous diffusion equations in transition region between Knudsen and molecular diffusion. *Ind. Eng. Chem. Fundam.*, 9, 206–210. DOI: 10.1021/i160034a003.

Remick R.R., Geankoplis C.J., 1974. Ternary diffusion of gases in capillaries in the transition region between Knudsen and molecular diffusion. *Chem. Eng. Sci.*, 29, 1447–1455. DOI: 10.1016/0009-2509(74)80169-7.

Schiesser W.E., 1991. *Numerical methods of lines integration of partial differential equations.* Academic Press, San Diego.

Tabiś B., Bizon K. 2020. *Opracowanie metody linii do całkowania dynamiki dyfuzji wieloskładnikowej w materiałach makroporowatych*. Prace Katedry Inżynierii Chemicznej i Procesowej Politechniki Krakowskiej.

Tabiś B., Bizon K., 2018. *Dyfuzyjny ruch masy. Dyfuzja w gazach doskonałych i płynach rzeczywistych*. Wydawnictwa Politechniki Krakowskiej, Kraków.

Tabiś B., Boroń D., 2020. Application of the dusty gas model for determining structural parameters of porous media. *Przem. Chem.*, 99, 888–891. DOI: 10.15199/62.2020.6.11.

Tuchlenski A., Uchytil P., Seidel-Morgenstern A., 1998. An experimental study of combined gas phase and surface diffusion in porous glass. *J. Membr. Sci.*, 140, 165–184. DOI: 10.1016/S0376-7388(97)00270-6.

Veldsink J.W., Versteeg G.F., van Swaaij W.M.P., 1994. An experimental study of diffusion and convection of multicomponent gases through catalytic and non-catalytic membranes. *J. Membr. Sci.*, 92, 275–291. DOI: 10.1016/0376-7388(94)00087-5.

Yang J., Čermáková J., Uchytil P., Hamel C., Seidel-Morgenstern A., 2005. Gas phase transport, adsorption and surface diffusion in a porous glass membrane. *Catal. Today*, 104, 344–351. DOI: 10.1016/j.cattod.2005.03.069.

APPENDIX

The expressions for the first and second derivatives and the b_{mi} and g_{mi} coefficients are derived from orthogonal collocation rules (Finlayson, 1972). For the m^{th} collocation point, they are calculated as

$$\left.\frac{\partial \mathbf{p}}{\partial \xi}\right|_m = \sum_{i=1}^{M+2} b_{mi}\mathbf{p}_i\,, \qquad \left.\frac{\partial p}{\partial \xi}\right|_m = \sum_{i=1}^{M+2} b_{mi}p_i \tag{A1}$$

$$\left.\frac{\partial^2 \mathbf{p}}{\partial \xi^2}\right|_m = \sum_{i=1}^{M+2} g_{mi}\mathbf{p}_i\,, \qquad \left.\frac{\partial^2 p}{\partial \xi^2}\right|_m = \sum_{i=1}^{M+2} g_{mi}p_i \tag{A2}$$

$$\left[\frac{\partial}{\partial\xi}\mathbf{B}^{-1}\right]_m = \sum_{i=1}^{M+2} b_{mi}\mathbf{B}^{-1}(\mathbf{y}_i) \quad (m = 2, 3, \ldots, M+1) \tag{A3}$$

By applying relations (A1)–(A3), the partial differential equations (Eq. (18)) are transformed into a system of ordinary differential equations. For the m-th interior collocation point, we then get $K \times M$ of such equations

$$\varepsilon L^2 \left.\frac{\mathrm{d}\mathbf{p}}{\mathrm{d}t}\right|_m = \mathbf{F}_m(\mathbf{p}_m) \quad (m = 2, 3, \ldots, M) \tag{A4}$$

In expressions (A1)–(A3) $m = 2, 3, \ldots M+1$, M is the number of internal collocation points, while $\xi = z/L$ is a dimensionless spatial coordinate. Additional equations, at the ends of the integration interval $\xi \in [0, 1]$ i.e. for $m = 1$ and $m = M + 2$, are derived from the boundary conditions. Accordingly, provided that

$$\mathbf{p}(0, t) = \mathbf{p}_0 = \text{const} \tag{A5}$$

$$\mathbf{p}(1, t) = \mathbf{p}_L = \text{const} \tag{A6}$$

the extra equations are of the form

$$\left.\frac{\mathrm{d}\mathbf{p}}{\mathrm{d}t}\right|_{m=1} = 0, \qquad \left.\frac{\mathrm{d}\mathbf{p}}{\mathrm{d}t}\right|_{m=M+2} = 0 \tag{A7}$$

If the process proceeds in a closed diffusion cell (Fig. 2c), then the partial pressures of the components at boundaries $\xi = 0$ and $\xi = 1$ are determined from the balance equations (Eq. (15)). In terms of orthogonal collocation, we write them respectively as

$$\left.\frac{\mathrm{d}\mathbf{p}}{\mathrm{d}t}\right|_{m=1} = \frac{S}{LV_0}\left\{\mathbf{B}^{-1}\big|_{m=1} \cdot \left.\frac{\mathrm{d}\mathbf{p}}{\mathrm{d}\xi}\right|_{m=1} + \frac{\mathcal{B}_0}{\eta}\left.\frac{\mathrm{d}p}{\mathrm{d}\xi}\right|_{m=1} \mathbf{B}^{-1}\big|_{m=1}\mathbf{E}\cdot\mathbf{p}|_{m=1}\right\} \tag{A8}$$

$$\left.\frac{\mathrm{d}\mathbf{p}}{\mathrm{d}t}\right|_{m=M+2} = -\frac{S}{LV_L}\left\{\begin{array}{l}\mathbf{B}^{-1}\big|_{m=M+2} \cdot \left.\dfrac{\mathrm{d}\mathbf{p}}{\mathrm{d}\xi}\right|_{m=M+2} + \\ + \dfrac{\mathcal{B}_0}{\eta}\left.\dfrac{\mathrm{d}p}{\mathrm{d}\xi}\right|_{m=M+2} \mathbf{B}^{-1}\big|_{m=M+2}\mathbf{E}\cdot\mathbf{p}|_{m=M+2}\end{array}\right\} \tag{A9}$$

Received 02 June 2021
Received in revised form 21 July 2021
Accepted 27 July 2021